Influence of buried oxide layers of nanostructured SOI surfaces on matrix-free LDI-MS performances

Abderrahmane Hamdi, Ioana Silvia Hosu, Yannick Coffinier

Influence of buried oxide layer of nanostructured SOI surfaces on matrix-free LDI-MS performances.

Abderrahmane Hamdi, Ioana Silvia Hosu and Yannick Coffinier*

Univ. Lille, CNRS, Centrale Lille, ISEN, Univ. Valenciennes, IEMN, UMR CNRS 8520, Avenue Poincaré, BP 60069, 59652 Villeneuve d'Ascq, France.

*Corresponding Author: Yannick Coffinier, Phone: +33 320197987; Fax: +33 (0)3.62.53.17.01; E-mail: yannick.coffinier@univ-lille.fr

Keywords : *nanostructured SOI, BOX thicknesses, metal assisted chemical etching, mass-spectrometry, laser desorption ionization, peptides.*

Abstract :

In this paper, we report on the nanostructuration of the silicon crystalline top layer of different "home-made" SOI substrates presenting various buried oxide (BOx) layer thicknesses. The nanostructuration was achieved *via* one-step metal assisted chemical etching (MACE) procedure. The etched N-SOI substrates surfaces were then characterized by AFM, SEM and photoluminescence. To investigate their laser desorption/ionization mass spectrometry performances, the different surfaces have been assessed towards peptide mixtures. We have shown that the matrix-free LDI process occurred from surface heating after laser irradiation and was fostered by thermal confinement in the thin nanostructured Si surface layer. This thermal confinement was enhanced with the increase of buried oxide layer thickness till an optimal thickness of 200 nm for which the best results in terms of signal intensities, peptides discrimination and spot to spot and surface to surface variations were found.

Introduction:

Matrix-free laser desorption/ionization (LDI) process known as SALDI (surface-assisted laser desorption/ionization) has been developed to limit the background coming from adducts and fragments of organic matrices present in the low molecular mass region during matrix assisted laser desorption ionization mass spectrometry (MALDI-MS). The detection of small compounds, below 700 Da, is thus hampered when MALDI-MS is performed. SALDI process mainly uses nanomaterials made of semi-conductors, metals, metal oxides and carbon-based structures. They are presenting several advantages for the analysis of small compounds[1] : i) no need of co-crystallization of the analytes with organic matrix, thus suppressing the intense background from matrix peaks [2–4]. ii) simplicity of sample deposition and iii) better reproducibility of results. All these advantages make SALDI surface suitable for high throughput analyses and make possible their integration in lab-on-chip devices[5,6]. Moreover, by controlling their shape, morphologies, porosities and dimensions (particles, nanowires…) their optical, electrical and thermal properties can be tuned for SALDI-MS applications[1,7]. From decades, SALDI surfaces presenting different shape and dimensions such as 0D (particles), 1D (nanowire/nanotubes) or 2D films (graphene, MoS_2) have been tested as LDI materials[8–11]. Recently, a new class of plasmonic metal materials has emerged as LDI-MS substrates. Indeed, gold particles, mesoporous organosilica@Ag janus particles or magnetic@SiO_2@Ag particles have shown very promising applications for the detection of nutrients, cervical and lung cancers and bacterial metabolism analysis.[12–17] However, porous silicon is still one of the most SALDI materials used, notably due to its high specific surface area, straightforward preparation, UV absorption, anti-reflective and low thermal properties (heat confinement) (see table 1)[18].

The matrix-free LDI process is mainly based on thermal driven mechanism. It comprises several occurring concomitant phenomena such as energy absorption (from laser), desorption and ionization steps[19]. So, to perform SALDI-MS analyses, the interfaces should be a good photon absorbent at λ=355 nm (laser wavelength with photon energy value of 3.49eV)[19]. Then, *via* non-radiative recombination of electrons and holes (heat dissipation *via* phonons), the desorption/ionization of analytes can take place. It's well known that surfaces morphology, dimension, porosity, density and periodicity are sturdily related to their physical properties such as optical absorption and thermal dissipation[20]. By tuning the nanostructures' dimension, a better control of the LDI performances is expected. Kim *et al.*, have recently shown that commercial SOI substrate can be used as SALDI surface for the MS detection of insulin[21]. In this study, authors have demonstrated that the laser energy is trapped into the thin top active silicon layer supported by a thermal insulator material (SiO_2). This buried oxide (BOx) presents a lower thermal conductivity ~ 1.3 $Wm^{-1}K^{-1}$ *vs* ~40-60 $Wm^{-1}K^{-1}$ for top silicon layer (thicknesses of 50-100nm) (following the Fuchs-Sondheimer model) that is to be

compared to thermal conductivity value of 150 $Wm^{-1}K^{-1}$ for bulk Si[22]. The presence of underlying insulator material may provide an effective heat diffusion barrier which enables the energy to stay confined within the thin surface layer with low thermal conductivity, promoting heat confinement. In addition, it's well known that the porosification drastically decreased the thermal conductivity of silicon nanostructures[23,24].

So here, what we propose is to take advantage of the nanostructuration of the silicon layer of SOI substrate *via* metal-assisted chemical etching (MACE) method to obtain a low thermal conductive surface (N-SOI) for LDI-MS detection of small compounds. By doing so, lower laser fluence to perform LDI process is expected. As model compounds, we choose calibration peptides and antibiotics.

II) Materials & Methods

a) Materials

Silicon wafers have been purchased from Sil'tronix Silicon Technologies (Archamps, France). All cleaning and etching reagents were of VLSI grade. Sulphuric acid, 96% (H_2SO_4) from Technic (France), hydrogen peroxide 30% (H_2O_2) and nitric acid 65% (HNO_3) from Carlo Erba, hydrofluoric acid 50% (HF) and ammonium fluoride (NH_4F) were supplied by BASF. Silver nitrate ($AgNO_3$), acetone, hexane, dichloromethane (CH_2Cl_2), trifluoroacetic acid (TFA), ammonium citrate dibasic, methanol (MeOH), isopropyl alcohol (IPA) and ethanol (EtOH) were purchased from Sigma-Aldrich. Otcadecyltrichlorosilane (OTS) was purchased from ABCR (Germany). Peptide mixtures were obtained from Applied biosystem. An ultrapure water (Milli-Q, 18 MΩcm) system was used for solutions preparation and rinsing steps.

b) Nanostructures fabrication

The nanostructuration of the c-Si top layer of the home-made SOI surface was achieved by chemical etching in $NH_4F/HNO_3/AgNO_3$ aqueous solution[25,26]. Home-made SOI substrates were fabricated as follow: The silicon surface ((100), p-type, low resistivity) was cleaned in subsequent baths of acetone and isopropyl alcohol, followed by a rinsing step in MilliQ water. Then, the surface was plunged in a piranha solution (H_2SO_4/30% H_2O_2; 1/1 (v/v)) during 20 min at RT, followed by copious rinsing with Milli-Q water. The clean silicon surfaces were then thermally oxidized in a Low Pressure Chemical Vapor Deposition (LPCVD) furnace (Tempress) by using a well calibrated process. The thicknesses of the oxidized silicon were measured by ellipsometry (Horiba Jobin Yvon). 5 thicknesses were obtained with the following values: 0, 50, 100, 200 and 400 nm of SiOx. Then, 150 nm of a crystalline silicon layer was deposited by Low Pressure Chemical Vapor Deposition. The thickness was measured by ellipsometry and confirmed by SEM cross-view measurement. For the nanostructuration of SOI surfaces, they were dipped in $NH_4F/HNO_3/AgNO_3$ (6.00 M/5.73 M/0.02 M) aqueous solution at room temperature during various times: from 10 s to 5 min, then followed by a copious rinsing step with deionized water. To ensure the complete removal of silver dendrites formed during the chemical

etching, the surfaces were immerged in HNO_3 (65%) during 10 min. Finally, the nanostructured SOI (N-SOI) surfaces were copiously rinsed with deionized water and dried under a stream of nitrogen. It has to be noticed that the same process was applied on crystalline Si wafer noted N-cSi. SOI (un-structured) and N-cSi surfaces were used as references.

Safety considerations

H_2SO_4/H_2O_2 (piranha), an exothermic solution that can react with organic chemicals and cause severe skin burns. It must be manipulated with extreme care under fume hood while operators should wear appropriate individual chemical safety protection.

Fluorhydric acid (HF) can result in serious tissue damage, even death. It should be handled in a well-ventilated fume hood with appropriate individual protection.

c) Silanization of surface by octadecyltrichlorosilane (OTS)

All surfaces were submitted to UV/ozone treatment (UV-O Cleaner, Jelight Company, Inc., 4mW/cm^2 at 220 nm) during 15 min to generate silanols groups (activation). Then, the surfaces were plunged in 10^{-3} M solution of OTS in hexane during 4h at room temperature in a dedicated glovebox[25–27]. The surfaces were then rinsed with CH_2Cl_2, isopropyl alcohol and dried by a stream of nitrogen.

d) Characterization of interfaces

Scanning electron microscopy (SEM)

SEM images were obtained using an ULTRA 55 (Zeiss) electron microscope equipped with EsB, high efficiency In-lens SE and Everhart-Thornley Secondary Electron detectors and an energy dispersive X-ray analysis device (Brüker) for EDX measurements.

Atomic force microscopy

Atomic Force microscopy (AFM) imaging was achieved in the tapping mode with a Dimension 3100 Model AFM (Veeco, Santa Barbara, CA) with a Nanoscope IV controller from Digital Instruments under ambient conditions. Silicon cantilevers (Nanoworld) with spring constants of 42 Nm^{-1} and resonant frequencies between 250 and 400 kHz were used.

Photoluminescence measurement

Photoluminiscence spectra have been recorded at 351.1 nm (argon laser (P=10 mW)) at room temperature by using an IHR 320 spectrometer from HORIBA Jobin Yvon. A 10× microscope objective was used for both producing a beam waist of 0.5 µm and collecting the backscattered PL light from samples. A 360 nm emission cutoff filter was used during measurements.

Reflectivity measurement

An UV-vis spectrophotometer from Perkin-Elmer (with an integrating sphere) was used for measuring sample reflectance. Spectra were registered between 200 and 800 nm at an incident light angle of 45°.

Contact angle measurements

A goniometer system DIGIDROP (GBX, France) was used for measuring the water contact angles. All measurements were performed by using a water droplet of 1µL. All measurements have been done in clean-room facilities environment. All presented values are average of 4 measurements done on different surface locations.

e) LDI-MS analysis

An Ultraflex TOF/TOF instrument (Bruker Daltonics, Wissembourg, France) with a pulsed Nd:YAG laser (λ=355 nm at 100 Hz) was used. All mass spectra were acquired in the positive and reflectron modes. The laser fluence was adjusted for each experiment and ions were detected from m/z 800 to 6500. The S/N threshold was fixed at 3 for better reliability. Data acquisition and processing were achieved with Flex Control and Flex Analysis softwars, respectively. Instrument calibration was achieved prior each experiment. N-SOI interfaces were fixed on stainless-steel MTP TLC adapter (Bruker) with a conductive tape and directly introduced into the mass spectrometer ion source. All experiments were repeated at least three times to ensure better reproducibility.

d) Peptide solutions

The peptide solutions were composed by: i) Des-Arg1-Bradykinin m/z 904.05; Angiotensin I m/z 1296.51; Glu1-Fibrinopeptide B m/z 1570.61; Neurotensin m/z 1672.96 (solution 1) and ii) ACTH (clip 1–17) m/z 2094.46; ACTH (clip 18–39) m/z 2466.72, ACTH (clip 7–38) m/z 3660.19 and Insulin m/z 5734 (solution 2). All peptides were resuspended in water/acetonitrile 50/50 at 25 pmol/µL in presence of 0,3% TFA. Before each SALDI-MS experiment, peptide solutions were diluted in ammonium citrate (1mM) at the desired concentration (5pmol, 500 fmol and 50 fmol). Then, 0.5µl was deposited on N-SOI surface and let dried at room temperature under ambient atmosphere.

III- Results and discussion

Morphology of the SALDI surface is crucial in the matrix-free LDI processes. Indeed, it is known that interactions of nanostructured materials (dimensions <500 nm) with laser irradiation lead to more efficient desorption and ionization of compounds of interest[20]. This can be explained by the fact that for such nanostructures' dimensions, optical absorption and thermal dissipation are enhanced[20]. From this, we took advantages of the SOI substrate features *i.e.* thin layer of crystalline Si layer supported on buried silicon oxide layer and its nanoengineering to finely control the LDI-MS performances.

In this study, we set up "home-made" SOI surface composed by an active silicon top layer of 150 nm with various thicknesses of BOx layer. So, 5 types of SOI were chosen showing various BOx thicknesses *i.e.* 0, ~50, ~100, ~200 and ~400 nm (**Figures S1 & S2**). Then, the fabrication of the nanostructured layer was achieved by submitting SOI substrates to MACE method as schematically represented on **figure 1**. In **figure 2** is represented SEM images of SOI substrate (BOx~200 nm) before

and after etching. After 10 seconds of etching, we can clearly see the nanostructures formation (slightly white by eye) with no decrease of the polysilicon or SiOx layers. Interestingly, for etching time greater than 10 seconds, the Si dissolution seems to take place laterally (**Figure S3**). Indeed, longer times of etching led to bigger holes formation, until the total disappearance of the top silicon layer of SOI (5 min of etching) (**Figure S3**). In **figure S4** presented SEM images of crystalline Si wafer submitted to MACE process, noted N-cSi. AFM characterization gave rough mean square (RMS) values of 0.1 and 1.7 nm for SOI and N-SOI, respectively (**Figure 3**), thus showing the obvious increase of surface roughness after the chemical etching.

III-2 Optical characterizations

Anti-reflective property of our N-SOI surfaces is crucial since it will help them to maximize photons absorption from the laser irradiation. The total reflectivity spectra for both bare SOI and N-SOI surfaces have been recorded from wavelengths ranging from 250 to 800 nm (**Figure S5**). Both SOI (BOx=0nm) and N-SOI (BOx=0nm) surfaces present similar reflection spectra profile with lower reflectance for the etched one due to lower refractive index (**Figure S5**)[28]. For other SOI surfaces with BOx=50, 100, 200 and 400 nm, reflection spectra are quite different and are divided in two zones, a metallic-type reflection at small wavelengths <425 nm and Fabry-Perot cavity type reflection (fringes) at lower wavelengths, typical of SOI substrate and mainly due to reflections at the Si/SiO_2 interfaces (**Figures 4 and S5**)[29]. After etching, a reflectance reduction (increase light absorption) is observed that can be attributed to the strong light scattering and diffraction occurring at the nanostructured interfaces (**Figures 4 and S5**). To summarize, by achieving chemical etching of SOI surface, we increased the surface porosity, leading to better anti-reflective properties (30% of reflectivity for N-SOI *vs* 45% for SOI) at 355 nm (wavelength used for LDI-MS) for all considered BOx thicknesses. This better anti-reflective property makes N-SOI better photon absorber than bare SOI surface thus suggesting a better energy transfer that can take place, from N-SOI surface to analytes during LDI process[30].

Moreover, the laser penetration depth in the silicon nanostructures at the considered wavelength (λ=355 nm) is lower than 100 nm, by taking into account the nanostructure optical absorption and reflection in this energy range. As the thin nanostructured active silicon layer is ~150 nm, we can expect an exclusive photon absorption by the top layer during pulsed laser irradiation. In addition, in the case of SALDI surfaces, analytes have to be uniformly distributed within the nanostructured layer to be efficiently desorbed. Indeed, it was noticed that when the thickness of a porous silicon layer is too high, analytes could be trapped deeply inside the nanostructured layer[27,31]. Then, albeit the energy was accordingly transferred to analytes, the desorption phenomenon could be less efficient with as main consequence, a decrease of the detection sensitivity. In our case, analytes deposited on N-SOI will be well distributed and won't have the possibility to go deeper because of the underlying

SiO_x. Finally, the presence of SiO_x underneath the nanostructured silicon layer will enhance the heat confinement inside the nanostructured silicon layer after laser irradiation, improving the efficiency of the LDI-MS process.

The photoluminescence measurements were also performed of both surfaces and spectra are displayed in **figure 5**. The excitation wavelength was fixed at 351 nm. We can observe a broad PL spectrum from 450 nm to 900 nm for both substrates. By comparing both intensities, no increase of PL was observed, meaning that no quantum confinement occurred after etching. However, a centered peak at 625 nm for the N-SOI substrate (BOx 200 nm, blue curve) which is blue-shifted (~675 nm) compared to PL obtained from SOI substrate (BOx 200 nm, black curve). This is a further indication that the PL originates from surface defects and from the silicon oxide layer[32]. We can then postulate that the adsorbed energy will be mainly dissipated by non-radiative mechanism, leading to heat generation[33].

III-3 Chemical modification & LDI-MS applications

III-4-1 Water contact angle (WCA) measurements

The freshly prepared N-SOI surfaces present superhydrophilic behaviors with water static contact angle (WCA) values of ~0°, that is mainly due to the presence of the native oxide layer around the nanostructures. In that case, when a liquid droplet, containing the analytes, is deposited onto the surface, it will entirely wet the surface. To better control the wetting properties and to avoid the droplet spreading, we have chemically functionalized the different surface with octadecyltrichlorosilane (OTS). For the N-SOI surfaces, we obtained WCA values of 125° after silanization. To compare, the WCA values obtained for the OTS-terminated from un-structured SOI and nanostructured crystalline Si (N-cSi) were 108° and 123°, respectively (**Figure S6**). Such WCA values of ~125° is known to be suitable for good and reproducible analyte deposition[25].

III-3-2 Peptide MS detection

To go further, we have assessed the ability of our nanostructured SOI surfaces to perform LDI-MS detection of peptides. To do so, after their chemical modification by OTS, 0.5µL of peptide solution was deposited and let dried on each surface to be tested *i.e.* SOI, N-SOI and N-cSi. It has to be noticed that each deposition was done 3 times on same surface (3 spots) and 3 surfaces of each type were tested to check the reliability of the conducted experiments. Their performances were then evaluated in term of peptide discrimination (number of peptides detected/number of peptides in the mixture), signal intensities and laser fluence used. We started with the lower laser fluence and increase gradually until to obtain all peptides detected when possible. In **figure S7**, it's shown the mass spectrum cleanliness obtained on N-SOI (Box 200 nm) surface compared to the one acquired with α-cyano-4-hydroxycinnamic acid (CHCA).

N-SOI surfaces with different BOx thicknesses were first tested against 2 peptides solutions. Solution 1 composed by Des-Arg^{1}-Bradykinin m/z 904; Angiotensin I m/z 1296; Glu^{1}-Fibrinopeptide B m/z 1570; Neurotensin m/z 1673 (peptide mixture 1) and solution 2 composed by Angiotensin I m/z 1296; ACTH (clip 1–17) m/z 2094; ACTH (clip 18–39) m/z 2466; ACTH (clip 7–38) m/z 3660 and Insulin m/z 5734.

In **figure S8** are presented mass spectra for peptide solution 1 deposited on N-cSi and N-SOI (BOx=0nm) surface and then detected by SALDI-MS. We can see huge difference between the 2 spectra with low signal intensities for N-cSi and only 2 on 4 peptides detected. N-SOI (BOx=0nm) showed higher signal intensity and good peptide discrimination (4 on 4 are detected). Despite the 2 surfaces were etched under the same conditions, they presented significant difference in terms of LDI-MS performances. One explanation could be that they have different thermal conductivities. Indeed, heat conduction in silicon is dominated by phonon transport. The N-SOI (BOx=0nm) thermal conductivity is reduced compared to that of N-cSi due to more important scattering mechanisms in the thin layer that are not present in the bulk material. Indeed, the reduction is more severe and extends to higher temperatures for thin layers than for bulk samples. Also important is phonon scattering on imperfections or grain boundaries, which exist in larger amount in SOI substrates compared to bulk material[34]. This phenomenon is amplified by structuring the thin layer thus enhancing the phonon scattering and lowering the thermal conductivity of N-SOI (BOx=0nm). A thermal conductivity for a porous silicon layer with a thickness of ~200 nm was measured to be 1.7 $Wm^{-1}K^{-1}$ [24].

When buried oxide layer with various thicknesses (50, 100, 200 and 400 nm) are present between the nanostructured active layer and bulk Si, we can see that all N-SOI surfaces are able to detect all peptides present in the solution 1 (**Figures S9 and 6A**). For each peptide from solution 1, almost same signal intensities' profile in function of BOx film thickness is observed with a significant increase of the signal intensities for N-SOI (BOx=200 nm) whereas a significant decrease is observed for BOx thickness of 400 nm (**Figure S10**).

From **figure S10 and table S1**, we can notice that for Glu^{1}-Fibrinopeptide B and Neurotensin, their signal intensities and S/N are lower than for Des-Arg^{1}-bradykinin and Angiotensin I. We know from previous study that SALDI-MS detection of peptides with masses superior to 1200 Da is more difficult to perform[25]. It has to be noticed that Glu^{1}-Fibrinopeptide B is 5 times less concentrated in the mixture compared to others. Moreover, some peptides could be averse to be desorbed and ionized when present as part of mixtures even if they showed good MS data when they were analyzed as pure solution[26]. This could explain the high variation of signal intensities for Glu^{1}-Fibrinopeptide B and Neurotensin. Nevertheless, this variation is lower for higher BOx thickness *i.e.* 200 and 400 nm.

We have also tested another peptide mixture (solution 2) composed by 5 peptides with higher masses (**Figures 6B and S11**). We can observe that only one type of N-SOI with BOx thickness of 200 nm is able to detect all the peptide with relevant intensities. Again, for all peptides considered within this work, the N-SOI (200nm) has shown the best LDI-MS performances in terms of peptide discrimination, signal intensities, S/N and spot to spot and surface to surface variations (**Figure S12 and table S1**). Concerning the LoD, the intensity profiles were recorded at 5pmol, 500 fmol and 50 fmol for each peptide solutions. Under our experimental conditions, an optimal detection at 10^{-6} M including signal intensities and peptide discrimination for peptide solution 1 and 10^{-5} M for peptide solution 2 were observed. However, at lower concentrations (such as 50 fmol), some peptides are very difficult to detect as mixture although they gave good data when analyzed in pure form.

In the contrary, we can notice that for N-SOI, with BOx thickness of 400 nm, a drastic decrease of signal intensities for all peptides considered in this study. A tentative explanation of this phenomenon could be drawn by the fact that by increasing the thickness of the thermal insulator, we decrease the thermal diffusivity (heat moves less rapidly). As a consequence, the surface will maintain a certain level of temperature (no rapid cooling) promoting the increase of peptide fragmentation thus decreasing the signal intensities of peptides (**Figures S10 and S12**). It was shown that there exists a tiny frontier between desorption and fragmentation and that the faster is the increase of the temperature, the lower is the fragmentation .[Erreur ! Signet non défini.] In the case of BOx=400 nm, the lower thermal diffusivity can keep the surface at a certain temperature thus promoting the peptide fragmentation.

As a control, a non-structured SOI surface (BOx = 200nm) was modified by OTS and then used for the LDI-MS detection of peptide solution 1 (**Figure S13**). The non-structured SOI surface only permitted the detection of 2 on 4 peptides at 40 % laser fluence with lower signal intensities values than all N-SOI independently of BOX thickness. More interestingly, even at low laser fluence, *i.e.* at 2% of laser fluence (instrument parameters), all peptides from peptide solution 1 have been detected when N-SOI (BOx=200 nm) surface was used (**Figure S14**). The use of low laser fluence will ensure the limitation of analytes fragmentation. In the contrary, when too high laser fluence was used, the thin nanostructured silicon active layer was completely ripped off as we can see on the SEM images (**Figure S15**).

We also performed the detection of model peptides spiked in serum to check the ability to detect peptides from complex solution. To do so, we made a solution 1 (1µL of Solution 1 in 24 µL of pure serum) and then deposit 0.5 µL of the mixture during 10 minutes. Then, the droplet was withdrawn and the remaining liquid let dried under ambient atmosphere prior MS detection. On **figure 7**, we can observe that all peptides from solution 1 were detected even when they are present in complex medium.

Finally, and to demonstrate that our N-SOI can also detect other type of compounds, antibiotics have been tested. It's well known that they are involved in current public health crisis because of their abusive use or misuse in food, animals or human treatments. In this extent, their SALDI-MS detection could be an interesting alternative of the classical current methods *e.g.* microbiological or immunoassays[35]. To do so, 4 antibiotics such as kanamycin m/z 484.5; novobiocin m/z 612.6; apramycin m/z 539.6; and erythromycin m/z 733.9 have been investigated at concentration of 100 µg/mL in pure or mixed solution (equimolar concentration) in presence of 10 mM NaCl. All antibiotics appeared in mass spectra in their protonated, sodiated or potassiated forms in both pure and mixed solutions (**Figures S16 and S17**).

IV- Conclusions

In this paper, we present the nanostructuration of the active top layer of SOI substrate *via* one-step MACE method. The fast preparation <1hour that includes 10 sec of etching and 30 min of chemical functionalization was sufficient to uniformly nanostructure the top active silicon layer of the SOI surface and use as SALDI surface. To investigate the influence of the BOx layer thickness on the LDI performances, we realize "home-made" SOI surface made of bulk silicon covered by various thicknesses of oxide and a thin layer of polysilicon (150 nm), both achieved *via* LPCVD.

The LDI-MS performances of the resulting surfaces were then assessed towards peptides and antibiotics mixtures and compared to references *i.e.* non-structured SOI surface and crystalline silicon structured using the same protocol. LDI-MS detection of peptides was successfully achieved on all tested surfaces with best results for N-SOI with a BOx thickness of 200 nm surface in terms of signal intensities, peptides discrimination and spot to spot and surface to surface variations.

We think that such nanostructured silicon layer is a very promising surface adaptable to any type of MALDI-ToF instrument and easy and fast to prepare. The good performances displayed at low laser fluence can also be useful in case of sensitive compounds limiting the risk of fragmentation. Also, application of such surface to mass spectrometry imaging (MSI) could be also considered. Indeed, the possibility to perform irradiation at sufficiently low laser fluence will help us preserving the biological content of the tissue by decreasing the ablation spot size, and so will increase the MSI resolution. Other important parameters are the thermal conductivity and heat diffusivity that will control the area corresponding to the tissue vaporization. So, N-SOI surface could a very relevant alternative to stainless steel, ITO or other metal substrates used in MSI.

Acknowledgments

The Centre National de la Recherche Scientifique (CNRS), the Lille University, the Hauts-de-France and the CPER "Photonics for Society" are acknowledged for financial support. I. S. H. acknowledges

the University Lille and DGA (Direction générale de l'armement, France) for PhD funding. The Renatech Network is also acknowledged for providing great support and technical conditions. This work was partly supported by the Ministry of Higher Education, Scientific Research and Technology of Tunisia.

Table 1 SALDI interfaces properties and their advantages *vs* MALDI

Surface properties	**Advantages/MALDI**
Optical properties: UV absorbent, Anti-reflectives	No organic matrices Simple deposition method, uniform distribution of analytes - No "hot spots"
Thermal properties: Low thermal conductivity, heat confinement	Low laser fluence- Limitation of fragmentation Low background
Chemical modifications : Reproductibility, Affinity capture, Activation energy	High specific surface area Great adsorption capacity of analytes
Other parameters influencing LDI performances : Porosity, dimensions, doping	Sensitive towards small compounds <10000 Da Salt tolerant, adaptable to any MALDI-ToF instrument

Figure captions

Figure 1: Schematic representation of the whole procedure to nanostructure Si based surfaces, their chemical modification and their use as SALDI surfaces for analytes MS detection.

Figure 2: SEM images comparing reference SOI and structured SOI achieved by MACE method for 10 sec of etching time.

Figure 3: AFM characterization for the comparison of reference SOI and structured SOI surfaces achieved by MACE method for 10 sec of etching time.

Figure 4: Reflectivity (R%) spectra measurements of the bare SOI and N-SOI (BOx=200 nm) (etching 10 sec) for wavelengths ranging from 250 to 800 nm.

Figure 5: Photoluminescence spectra of the bare SOI and N-SOI (etching 10 sec) in the wavelength range of (400–1100 nm) at room temperature.

Figure 6: MS spectra obtained from 2 peptides' solutions on N-SOI (BOx=200nm) substrate. Solution 1 (A) Des-Arg1-Bradykinin m/z 904; Angiotensin I m/z 1296; Neurotensin m/z 1673 at 50 fmol/µL and Glu1-Fibrinopeptide B m/z 1570 at 10 fmol/µL and solution 2 (B) Angiotensin I m/z 1296; ACTH (clip 1–17) m/z 2094; ACTH (clip 18–39) m/z 2466; ACTH (clip 7–38) m/z 3660 and Insulin m/z 5734 at 50 fmol/µL.

Figure 7: Mass spectrum showing the detection of all peptides in human blood serum sample. Spike of solution 1 Des-Arg1-Bradykinin m/z 904; Angiotensin I m/z 1296; Neurotensin m/z 1673 at 50 fmol/µL and Glu1-Fibrinopeptide B m/z 1570 at 10 fmol/µL in blood serum.

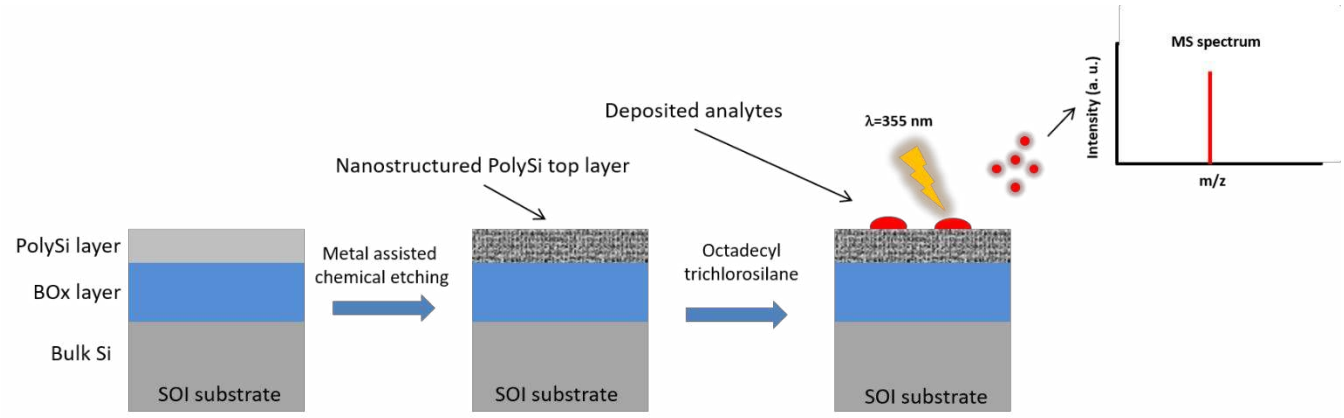

Figure 1: Schematic representation of the whole procedure to nanostructure Si based surfaces, their chemical modification and their use as SALDI surfaces for analytes MS detection.

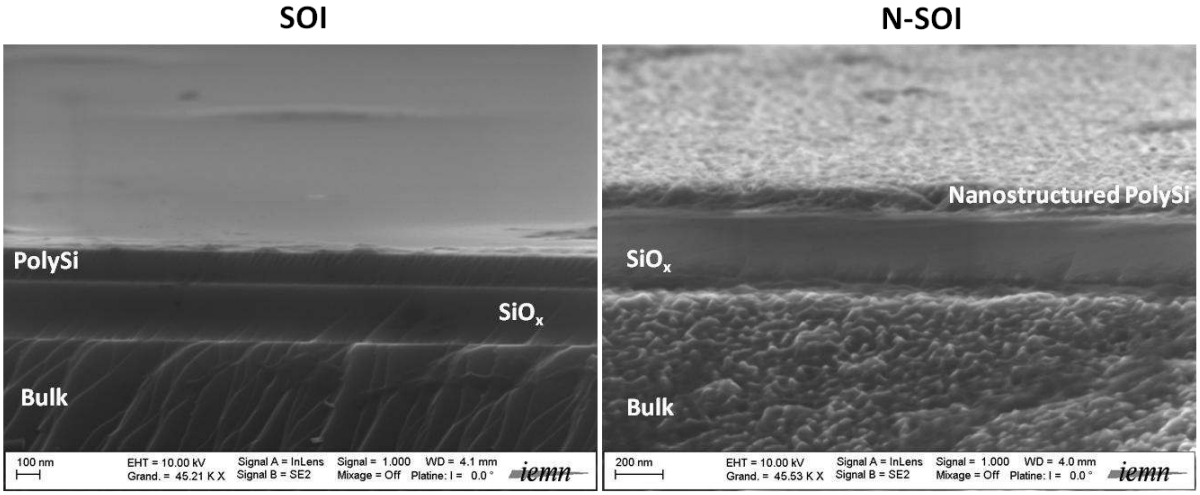

Figure 2: SEM images comparing reference SOI and structured SOI achieved by MACE method for 10 sec of etching time.

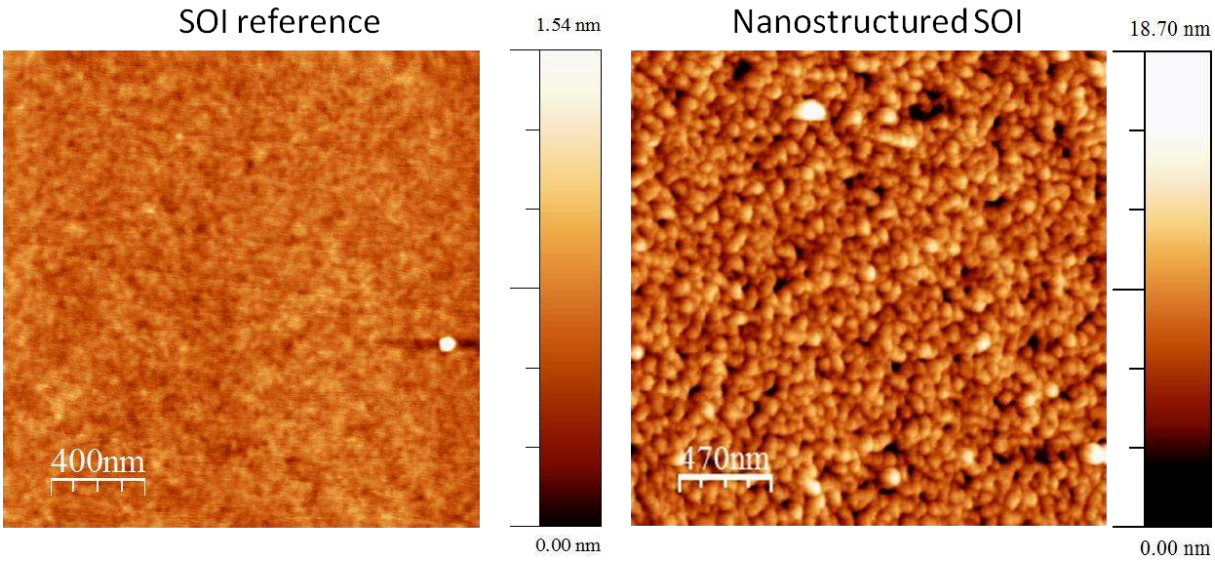

Figure 3: AFM characterization for the comparison of reference SOI and structured SOI surfaces achieved by MACE method for 10 sec of etching time.

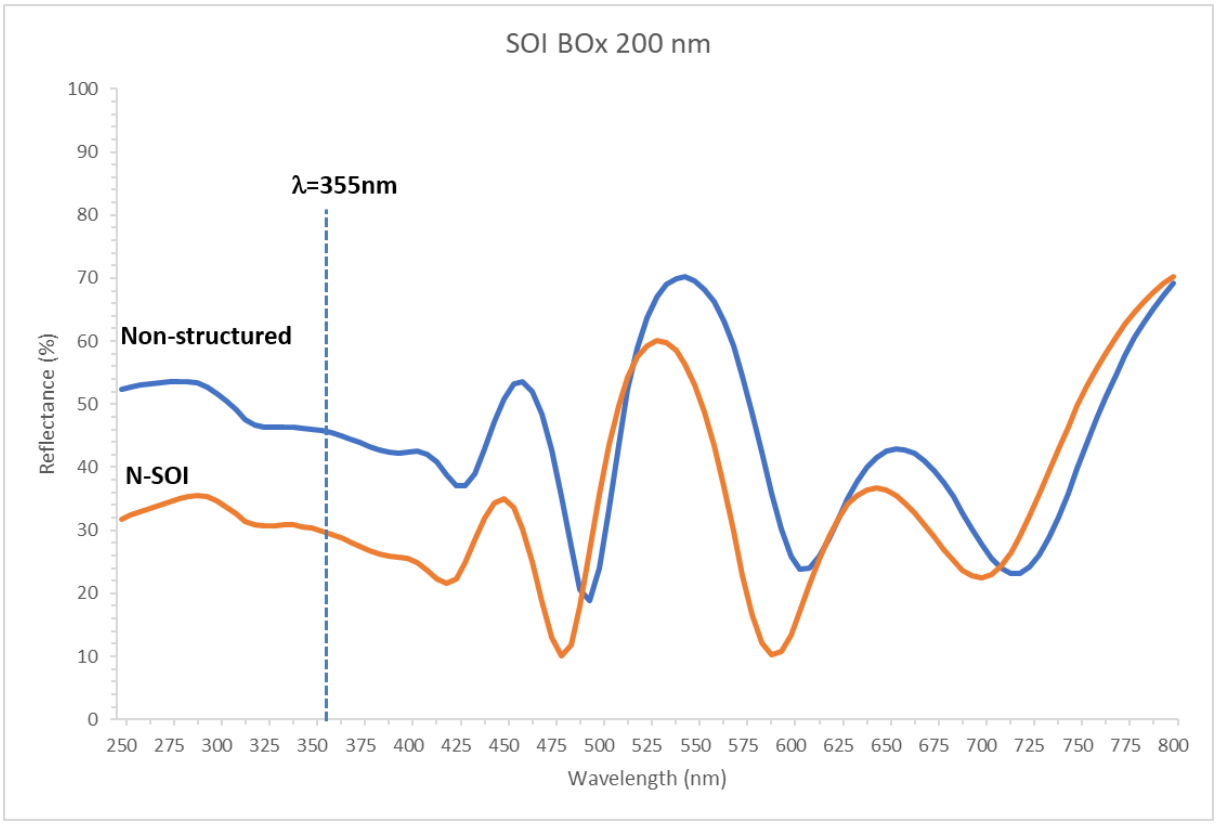

Figure 4: Reflectivity (R%) spectra measurements of the bare SOI and N-SOI (BOx=200 nm) (etching 10 sec) for wavelengths ranging from 250 to 800 nm.

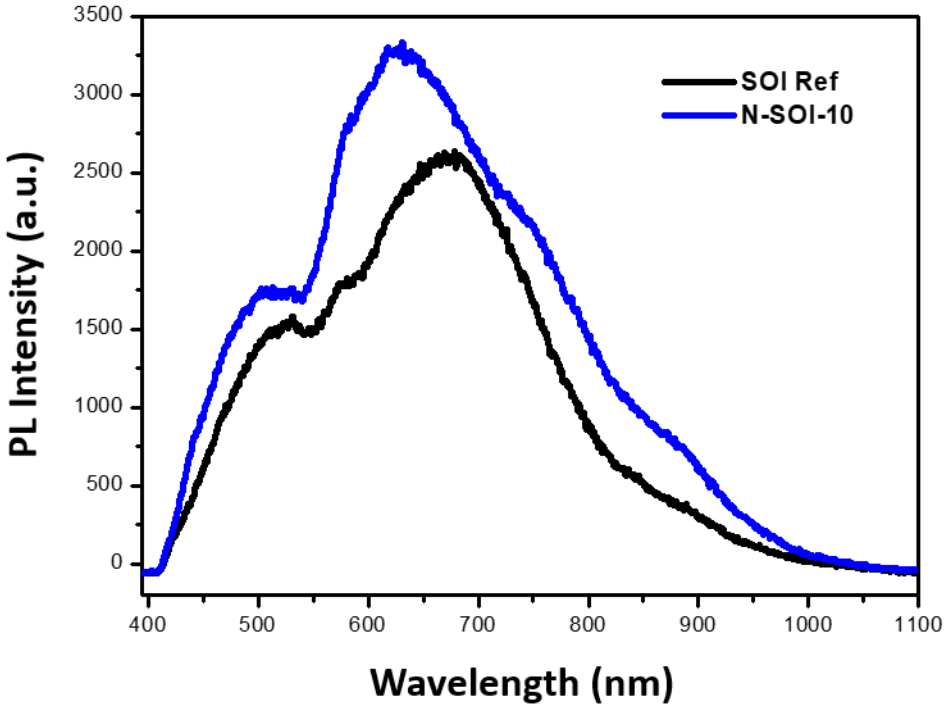

Figure 5: Photoluminescence spectra of the bare SOI and N-SOI (etching 10 sec) in the wavelength range of (400–1100 nm) at room temperature.

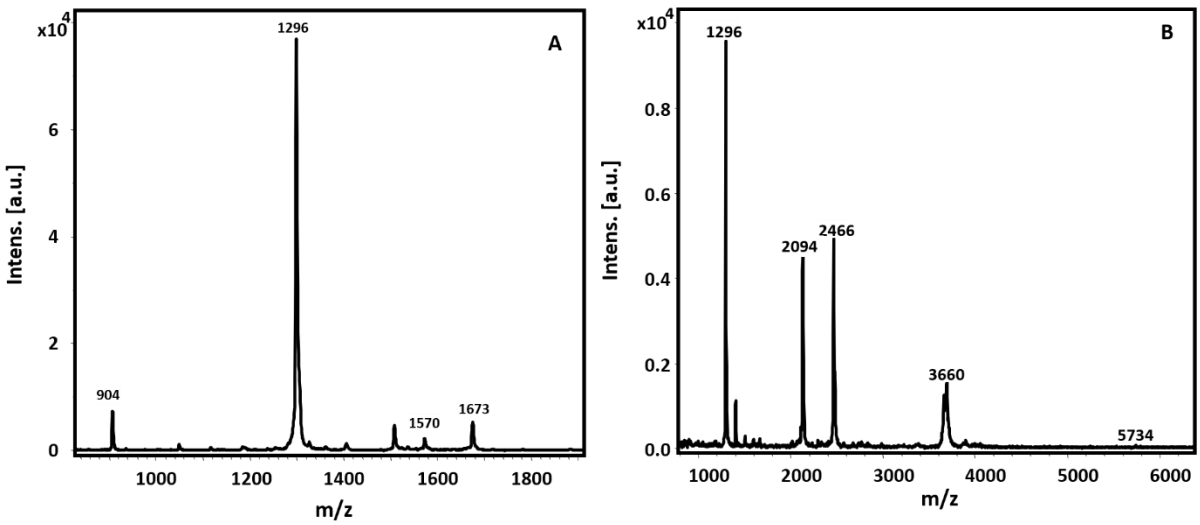

Figure 6: MS spectra obtained from 2 peptides' solutions on N-SOI (BOx=200nm) substrate. Solution 1 (A) Des-Arg1-Bradykinin m/z 904; Angiotensin I m/z 1296; Neurotensin m/z 1673 at 50 fmol/µL and Glu1-Fibrinopeptide B m/z 1570 at 10 fmol/µL and solution 2 (B) Angiotensin I m/z 1296; ACTH (clip 1–17) m/z 2094; ACTH (clip 18–39) m/z 2466; ACTH (clip 7–38) m/z 3660 and Insulin m/z 5734 at 50 fmol/µL.

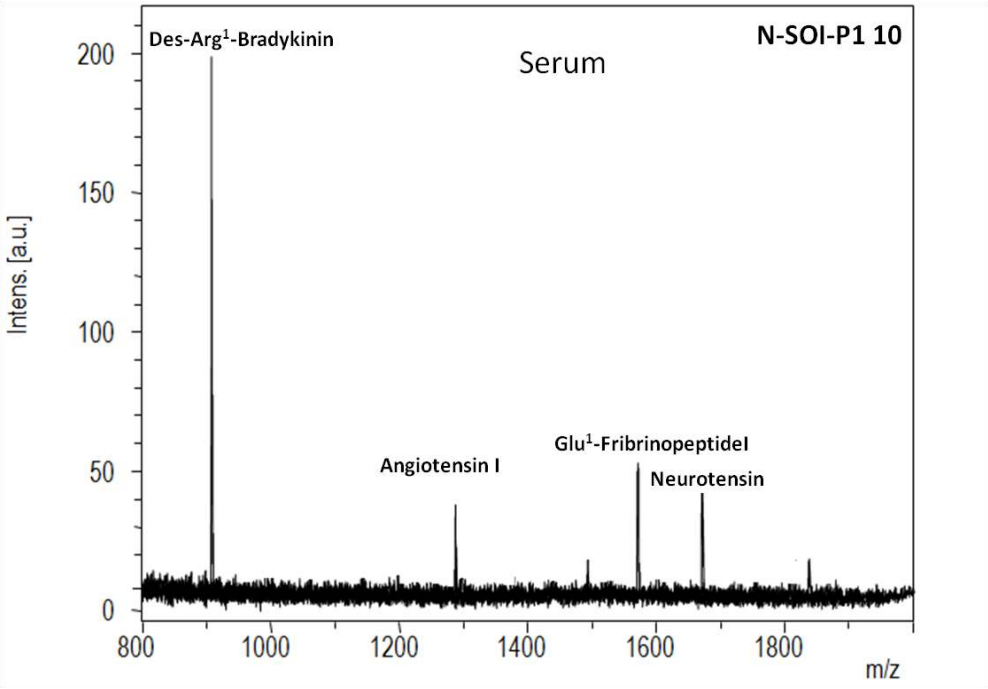

Figure 7: Mass spectrum showing the detection of all peptides in human blood serum sample. Spike of solution 1 Des-Arg1-Bradykinin m/z 904; Angiotensin I m/z 1296; Neurotensin m/z 1673 at 50 fmol/µL and Glu1-Fibrinopeptide B m/z 1570 at 10 fmol/µL in blood serum.

References

1 K. P. Law and J. R. Larkin, *Anal. Bioanal. Chem.*, 2011, 399, 2597–2622.

2 D. S. Peterson, *Mass Spectrom. Rev.*, 2007, **26**, 19–34.

3 S. Okuno, R. Arakawa, K. Okamoto, Y. Matsui, S. Seki, T. Kozawa, S. Tagawa and Y. Wada, *Anal. Chem.*, 2005, **77**, 5364–5369.

4 B. N. Walker, T. Razunguzwa, M. Powell, R. Knochenmuss and A. Vertes, *Angew. Chemie - Int. Ed.*, 2009, **48**, 1669–1672.

5 C. W. Tsao, S. Tao, C. F. Chen, J. Liu and D. L. Devoe, *Microfluid. Nanofluidics*, 2010, **8**, 777–787.

6 F. Lapierre, G. Piret, H. Drobecq, O. Melnyk, Y. Coffinier, V. Thomy and R. Boukherroub, *Lab a*

Chip, 2011, **11**, 1620-1628.

7 Y. E. Silina and D. A. Volmer, *Analyst*, 2013, **138**, 7053–7065.

8 C. Y. Shi and C. H. Deng, *Analyst*, 2016, **141**, 2816–2826.

9 S. A. Iakab, P. Rafols, M. García-altares, O. Yanes and X. Correig, 2019, **1903609**, 1–18.

10 Y. Coffinier, S. Szunerits, H. Drobecq, O. Melnyk and R. Boukherroub, *Nanoscale*, 2012, **4**, 231-238.

11 H. N. Abdelhamid, *Mikrochim. Acta*, 2019, **186**, 682.

12 W. Shu, Y. Wang, C. Liu, R. Li, C. Pei, W. Lou, S. Lin, W. Di and J. Wan, *Small Methods*, 2019, **1900469**, 1–9.

13 V. Vedarethinam, L. Huang, W. Xu, R. Zhang, D. D. Gurav, X. Sun, J. Yang, R. Chen and K. Qian, *Small*, 2019, **15**, 1–10.

14 X. Sun, L. Huang, R. Zhang, W. Xu, J. Huang, D. D. Gurav, V. Vedarethinam, R. Chen, J. Lou, Q. Wang, J. Wan and K. Qian, *ACS Cent. Sci.*, 2018, **4**, 223–229.

15 H. W. Chu, C. S. Lai, J. Y. Ko, S. G. Harroun, C. I. Chuang, R. Y. L. Wang, B. Unnikrishnan and C. C. Huang, *ACS Sensors*, 2019, **4**, 1543–1551.

16 H. Su, T. Liu, L. Huang, J. Huang, J. Cao, H. Yang, J. Ye, J. Liu and K. Qian, *J. Mater. Chem. B*, 2018, **6**, 7280–7287.

17 S. Wu, L. Qian, L. Huang, X. Sun, H. Su, D. D. Gurav, M. Jiang, W. Cai and K. Qian, *Nano-Micro Lett.*, 2018, **10**, 1–9.

18 E. P. Go, J. V. Apon, G. Luo, A. Saghatelian, R. H. Daniels, V. Sahi, R. Dubrow, B. F. Cravatt, A. Vertes and G. Siuzdak, *Anal. Chem.*, 2005, **77**, 1641–1646.

19 R. Zenobi and R. Knochenmuss, *Mass Spectrom. Rev.*, 1998, **17**, 337–366.

20 J. A. Stolee, B. N. Walker, V. Zorba, R. E. Russo and A. Vertes, *Phys. Chem. Chem. Phys.*, 2012, **14**, 8453–8471.

21 S. H. Kim, J. Kim, D. W. Moon and S. Y. Han, *J. Am. Soc. Mass Spectrom.*, 2013, **24**, 167–170.

22 K. Fuchs, *Math. Proc. Cambridge Philos. Soc.*, 1938, **34**, 100–108.

23 J. M. Weisse, A. M. Marconnet, D. R. Kim, P. M. Rao, M. A. Panzer, K. E. Goodson and X. Zheng, *Nanoscale Res. Lett.*, 2012, **7**, 1–5.

24 A. Melhem, D. De Sousa Meneses, C. Andreazza-Vignolle, T. Defforge, G. Gautier, A. Sauldubois and N. Semmar, *J. Phys. Chem. C*, 2017, **121**, 7821–7828.

25 M. Dupré, C. Enjalbal, S. Cantel, J. Martinez, N. Megouda, T. Hadjersi, R. Boukherroub and Y. Coffinier, *Anal. Chem.*, 2012, **84**, 10637–10644.

26 M. Dupré, Y. Coffinier, R. Boukherroub, S. Cantel, J. Martinez and C. Enjalbal, *J. Proteomics*, 2012, **75**, 1973–1990.

27 G. Piret, H. Drobecq, Y. Coffinier, O. Melnyk and R. Boukherroub, *Langmuir*, 2010, **26**, 1354–

1361.

28 L. Y. Chen, X. Y. Hou, D. M. Huang, P. H. Hao, F. L. Zhang, X. W. Feng, Y. H. Qian and X. Wang, *Jpn. J. Appl. Phys.*, 1994, **33**, 1937–1943.

29 G. Le and R. Romestain, 1997, **297**, 114–117.

30 R. Nayak and D. R. Knapp, *Anal. Chem.*, 2010, **82**, 7772–7778.

31 M. J. Kang, J. C. Pyun, J. C. Lee, Y. J. Choi, J. H. Park, J. G. Park, J. G. Lee and H. J. Choi, *Rapid Commun. Mass Spectrom.*, 2005, **19**, 3166–3170.

32 I. S. Hosu, M. Sobaszek, M. Ficek, R. Bogdanowicz, H. Drobecq, L. Boussekey, A. Barras, O. Melnyk, R. Boukherroub and Y. Coffinier, *Nanoscale*, 2017, 9, 9701-9715.

33 V. Lysenko, S. Perichon, B. Remaki, D. Barbier and B. Champagnon, *J. Appl. Phys.*, 1999, **86**, 6841–6846.

34 M. Asheghi, M. N. Touzelbaev, K. E. Goodson, Y. K. Leung and S. S. Wong, *J. Heat Transfer*, 1998, **120**, 30–36.

35 H. Sonderegger, C. Rameshan, H. Lorenz, F. Klauser, M. Klerks, M. Rainer, R. Bakry, C. W. Huck and G. K. Bonn, *Anal. Bioanal. Chem.*, 2011, **401**, 1963–1974.